ISSN: 2586-7652 (Print) Vol. 04, No. 02, September 2021
ISSN: 2635-7607 (Online)
International Journal of Advanced Engineering
Source: http://ictaes.org
Manuscript received: March 23, 2021; Revised: May 14, 2021; Accepted: May 22, 2021

A Review Study on Tensile Deformation and Hardening Behavior of Low-Density Steel

JV Muruga Lal Jeyan[1], Ankit Kumar Mishra[2],

[1,2]*Department of Aerospace engineering, Lovely Professional University, Punjab*

jvmlal@ymail.com[1], ankitkumarm1998@gmail.com[2]

Abstract

The low density steels plays a significant role in manufacturing as well as automobile industries promoting out for higher performance. The tensile properties and hardening behavior are the important factor to be considered for the evaluation of low structured steel, the study of different phase formations such as- martensite, austenite and κ-carbide elements and also reviewing the tensile properties, ultimate as well as yield strength, elongation point etc. The review study of this paper is to show the effect of microstructure developments and hardening behavior along with its mechanical as well as tensile properties, fracture characterization that will be responsible for the selection and manufacturing of respective steels.

Keywords: *Microstructures, Review, Hardening Behavior, Low-density steel*

1. Introduction

The low density steels plays a vital role in materials and manufacturing industries. The different classifications of low steels are made by mixing the compositions of different alloys such as- Aluminum, Manganese, Iron, Nickel, Carbon etc. The content of carbon is responsible for the transformation of phases and its constituents. The quality of steel is dependent on different mechanism followed by quenching, annealing, precipitating, tensile as well as mechanical tests, yield strengths. The content of aluminum shows the high strength, noble ductility and insubstantial properties. Similarly, the content of nickel and manganese strengthen the ductile properties of steel along with its fracture as well as yield strengths. Sufficient studies have been done for microstructures and mechanical properties on low density steels that are to be galvanized at different temperatures. The most advanced research is carried on steels for development of transformed induced plasticity (TRIP) as well as twin induced plasticity (TWIP) respectively. These steels also affect out the automobile as well as engineering industries

Corresponding Author : Ankit Kumar Mishra
Author's affiliation : Dept. of Aerospace Engineering, Lovely Professional University, Punjab
Email: ankitkumarm1998@gmail.com
Copyright © ICT-AES

responsible for weight reduction, cost reduction and increment in fuel efficiency.

2. Literature Review

Yang et.al studied the enactment of rigid distortion of low-density duplex Fe-Mn-Al-C steel. The experimental investigation was carried out using cast steel heating up to 1150 ◦C for certain amount of time. To evaluate the deformed dislocation structure, all samples were undergoing to a true strain using electronic universal testing machine. The Thermo-Calc software was also considered to study equilibrium phase diagram with the help of X-ray diffraction. The SEM optimization shows that the austenite matrix subjected to massive slip bands and the intersection for which deformation increases. The alteration in a way of strain hardening results in seamless arrangement of strength and ductility of Fe-Mn-Al-C steel. The grain subdivision characterized by micro-band intersection which relates to the stable performance of work hardening rate, and the continuous strain hardening behavior [1]. Li et.al studied the hot deformation and vigorous recrystallization actions of austenite based on low-density Fe-Mn-Al-C steel. The experimental investigation was carried out in such a manner that a solid block carrying bulk of 20 kg Fe-Mn-Al-C steel was made in vacuum induction furnace with different compositions. The stress flow cambers for the steel illustrates the DRX characteristics for amount of deforming temperature as well as strain rates. The yield point elongation effect is also observed and investigated with the use of heterogeneous strain lying between dual phases and δ-ferrite DRX. The presence of microstructure pattern was showed up by DRX for untested steel reflected on stage for clipping temperature and strain rates. The conclusion was made in way that increase in value of deformation temperature resulting in the decrease of strain rate and further leads in increment for austenite and δ-ferrite phase [2]. Zhao et.al investigated out the effect of hardening temperature on microstructure and ductile properties of Fe-10Mn-10Al-0.7C low density steel. The temperature range that was considered lies in range from 700- 1200 ◦C and the annealing specimens include out ferrite, austenite, and κ-carbide. A constituent phase was considered using X-ray diffraction analysis to analyze parameters for materials. The results of microstructures were observed using an optical microscope, field-emission scanning electron microscope. The tensile tests were carried out using universal testing machine for measuring stress as well as strain rate acting parallel to rolling direction. It is also observed that at annealing temperature the ductile properties are controlled by the fraction of austenite phase and the ultimate elongation and strength decreases with the increase in grain size [3]. Zhang et.al examined the ductile distortion appearance of Fe-Mn-Al-C low density steels for altered deformation conditions. The similar experimental was conducted for Li et.al and Zhao et.al in addition with the test steels inundated into lumps for heat treatment purposes at the temperature range of 1000-1100 ◦C. The microstructures and fracture analysis were studied under the several heat conditions and cooling modes. As of higher deformation rate, the shear omission of carbides is produced for which plasticity alloy decreases resulting to the SIP effect. Under several heat treatments and cooling conditions, ferrite and austenite were decomposed into $\alpha+\gamma+\kappa$ carbides as well as the mechanical properties were affected. It is observed that the decomposition kinetics of phase and diffusion rate of carbon accelerates the precipitation and improves the ductility of alloy but reduces the strength properties [4]. M. Zhang et.al established the element apportioning effect on microstructure and mechanical properties of micro-laminated Fe-Mn-Al-C phase steel. The phase ratios for these materials were calculated using Thermo-Calc software and an alloy design. The consideration of several factors was taken in the account for design phase such as- mechanical properties, temperature, density, strength, and plasticity etc. which results in an efficient way and led to the formation of the austenite phase during annealing process that is geared up with the help of first element partition [5]. Abedi et.al accomplished the frame hardening performance of Fe–17.5Mn–8.3Al-0.74C–0.14Si low-density steel. An experimental set up is arranged in such a way that the measurement of apparent density

is done using a densitometer. The evaluation for the piling fault energy is calculated on behalf of thermodynamic model that affect the content of materials with effect on grain size. The calculation for thermodynamic parameters is done by using Thermo- Calc software which confirms that material can hold the microstructures pattern when austenite phase is subjected to inclusive range of temperature. These experimental investigations validate the presence of ferrite phase along the boundary layers of the austenite which corresponds to an X-ray pattern [6]. Liu et.al studied the appliance of inter/intra-granular κ-carbides and its effect on overall mechanical properties of Fe-11Mn-10Al-1.25C low density steel. Few tests were carried out for which the studies were considered at microstructural levels and deformation mechanisms. A varied difference is observed in fracture modes of cooling outlines for which the sample is characterized by smooth surfaces and inter-granules shapes. The deformation for the experimented steel shows the activities of planar slides characterized by slip bands. The increase in work hardening rate of the sample displays the uniform property for nano-sized and shearable κ- carbides. It is also detected that overall tensile properties of the presented low density are highly expensive due to its high yield value and tensile strengths [7]. Alaneme et.al instigated the development of aluminum-based mixtures reinforced with steel and graphite-based particles based on physical, mechanical and wears representation. The Al-Mg-Si alloy was considered for experimental investigation and analysis as steel, graphite and silicon carbides were taken as the reinforcements for composite manufacturing. The composition and structural characterization were done on the basis of XRD analysis and scanning electron microscope (SEM). XRD analysis is considered to determine the crystalline phases and compositions produced for the selected alloy. In addition, analytical software is used for plotting of XRD peaks value and analyzing the diffraction phase parameters of samples. The microstructural and qualitative composite analysis is done with help of energy dispersive spectroscopy and secondary electron technique [8].

3. Discussion and Analysis

3.1 Microstructures Development

The variant samples were subjected to three different treatment processes- Air Cooling (AC), Water Quenching (WQ) and Intensive Quenching (IQ) that presents the study of precipitation behavior under notable conditions. The sample tests for an air cooling method, involves the study for grain boundaries whereas for water quenching and intensive quenching method, a chain structure is obtained for ferrite and κ- carbide elements subjected to an austenite matrix shown in Figure 1.

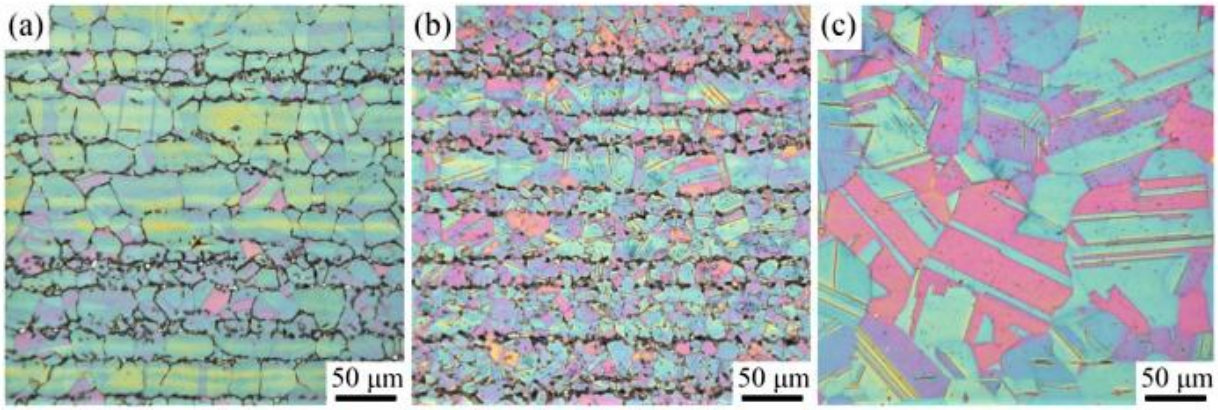


Figure 1. Optical graphs for Fe-11Mn-10Al-1.25C steel under (a) Air Cooling, (b) Water Quenching and, (c) Intensive Quenching [7].

On contrary, the IQ test samples were found relatable to grains and annealing clone's formation. The occurrence of κ carbides particles in AC process is found on behalf of peak values for austenite phase. The scanning electron microscopy (SEM) optimization led to the generations of two different phases for AC samples as one phase specifying about formation of thin film sheet of κ-carbide elements and other as to be dark grain layers which can be seen in figure 2. The dislocation occurrence is studied and analyzed for the formation of slip bands. The larger size and volume of κ-carbides elements indicates the probability for progressive risks in dislocations which correspondingly result to be under slip bands. The existence of ultra-high yield strength and ultimate tensile strength for AC samples occurs due to larger in size and volume of κ-carbides elements. It was also distinguished that increase in strain, the planar disorder is distinguished which endorse to the strain hardening.

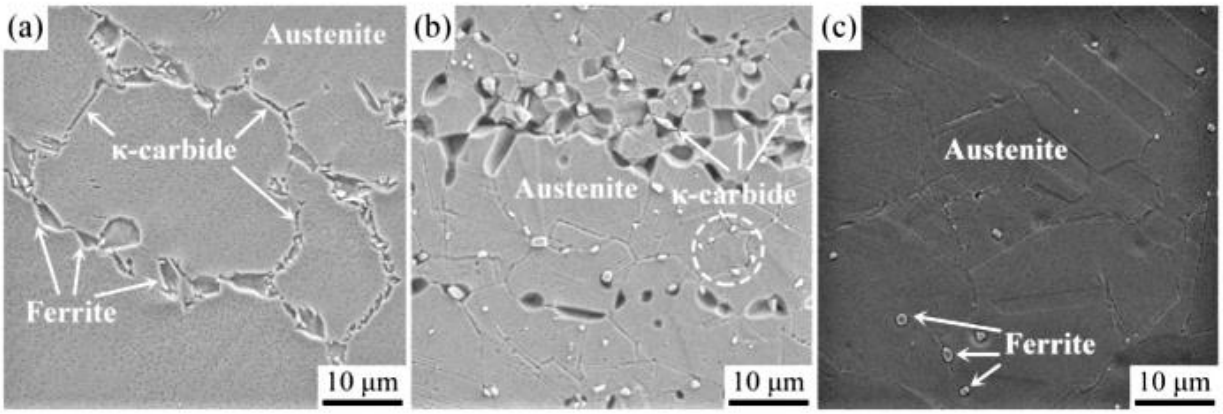


Figure2. SEM images of Fe-11Mn-10Al-1.25C steel for (a) Air Cooling, (b) Water Quenching and, (c) Intensive Quenching [7]

The transmission electron microscope estimation was also examined which results out to be the size range for κ-carbide particles are as 20 to 45 nm that is collected for air cooling samples and for water quenching as well as severe quenching it came out to be as less than 13 nm which is accountable for lattice reflection [7]. The dark images studied under TEM for a regular arrangement is shown in Figure 3.

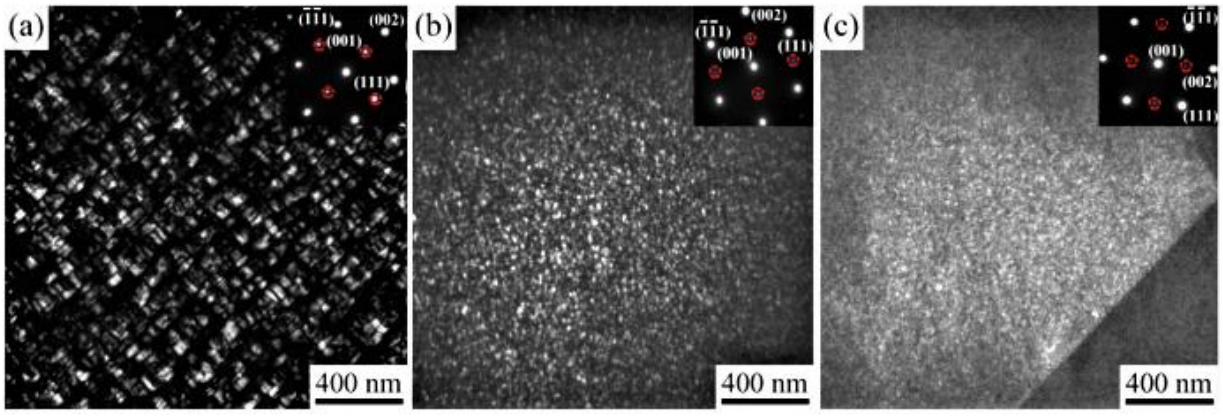


Figure 3. TEM images for steady arrangements of κ-carbide rational to austenite medium in Fe-11Mn-10Al-1.25C steel: (a) Air Cooling, (b) Water Quenching and, (c) Intensive Quenching [7].

The altitude difference between twofold phases caused in destruction under SEM can be seen brighter for ferrite phase as compared to austenite. The microstructure progress for specimen subject at different heights is displayed in Figure 4.

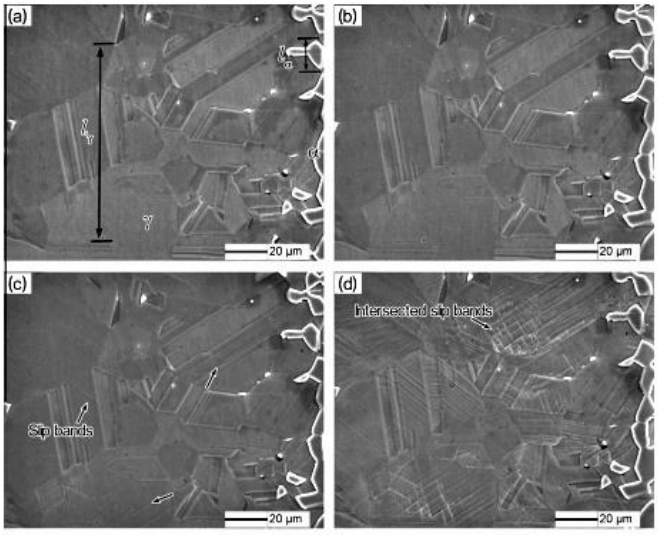


Figure 4. Microstructure images for different deforming displacements (a) at d = 0 mm; (b) at d = 0.5 mm; (c) at d = 0.8 mm; (d) at d = 1.4 mm [1].

It can be noted from figure 4(a) shows the microstructure grain at displacement, d = 0 mm representing at particular height. The figure 4(b) represents the elastic nature of deformation for slightly stretched out in the tensile direction for a subjected load for d = 0.5 mm. Further increasing the displacement at d = 0.8 mm, there is growth in subjected load and the occurrence of gliding dislocations are established resulting in the formation of grain layers for austenite as presented in figure 4(c). In figure 4(d), for d = 1.4 mm is shown the frontline progress of slip bands and its intersection due to growth in displacements. The scattering of slip bands of austenite particles for density increases for larger displacement in a range of 0.8 - 1.4 mm. The estimation for deformation of phases were calculated by using an equation described below-

$$\varepsilon = \ln (l_i/l_o) \quad (1)$$

Where, l_o is the actual distance between two points dignified for austenite and ferrite phase whereas l_i is the distance for displacements. A strain- displacement plot has been displayed below for two different phases i.e. austenite and ferrite for different displacement values.

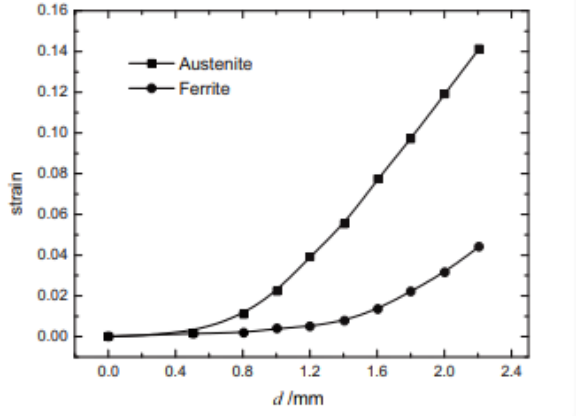


Figure 5. Strain Vs Displacement curve for austenite and ferrite phases [1].

From this plot it seems clearly that the austenite phase results in higher variation of strain with displacements than ferrite as the second phase of steel i.e. ferrite is subjected to lateral deformation in a rigid direction with an increase in distance [1]. The dynamic recrystallization (DRX) behavior is also analyzed under microstructure

expansion for which the temperature and strain rate were considered as major features. It was probed that with an increase in size for DRX grains, the temperature increases whereas strain rate decreases. The growth in size for DRX austenite and δ-ferrite transforms from a banded configuration into islet like at a strain rate fluctuating from 10 -0.01 s^{-1}. Optical images for temperature and strain rate are shown below investigated over different choice of temperatures. The images shown below represents at different temperatures and strain rate.

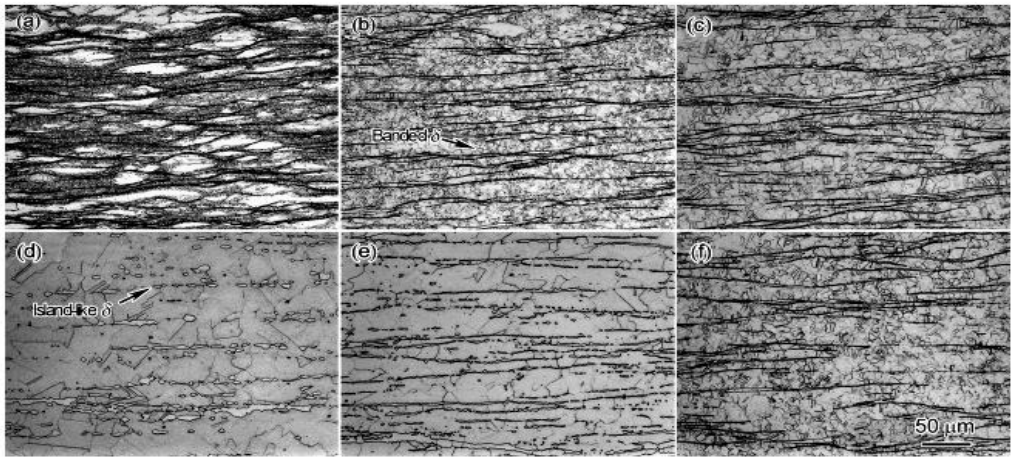


Figure 6. Optical microstructure for sample deformation under several temperature conditions a) at 900°C, b) at 1000°C, c) at 1100 °C, d) at 1100 °C, e) at 1100 °C, and f) at 1100 °C [2].

Figure 6 (a-c) expresses the difference for range of 900 - 1100°C at strain rate of 1 s^{-1}. With further increase of deformation temperature, the volume fraction as well as grain size increases. From figure 6 (d-f) the deformation is perceived at a temperature of 1100 °C for the strain rate of 0.01- 0.1 s^{-1} showing out consequences in austenite segment growth and edge region. The growth in deformation temperature also affects the low strain rate that endorses grain movement for austenite and δ-ferrite [2]. The XRD outcomes were supported out for κ-carbides components for temperature range 700- 850 °C. At 700 °C, the distribution for κ-carbide was not detectable as due to minor volume fraction or coherence of κ-carbide and α matrix. Lattice constraints were also estimated that varies from 2.89-2.91 Å, 3.65-3.67 Å for γ-phase and 3.76-3.79 Å for κ-carbide respectively. The optical microstructure images are displayed in Figure 7 at different annealing temperatures.

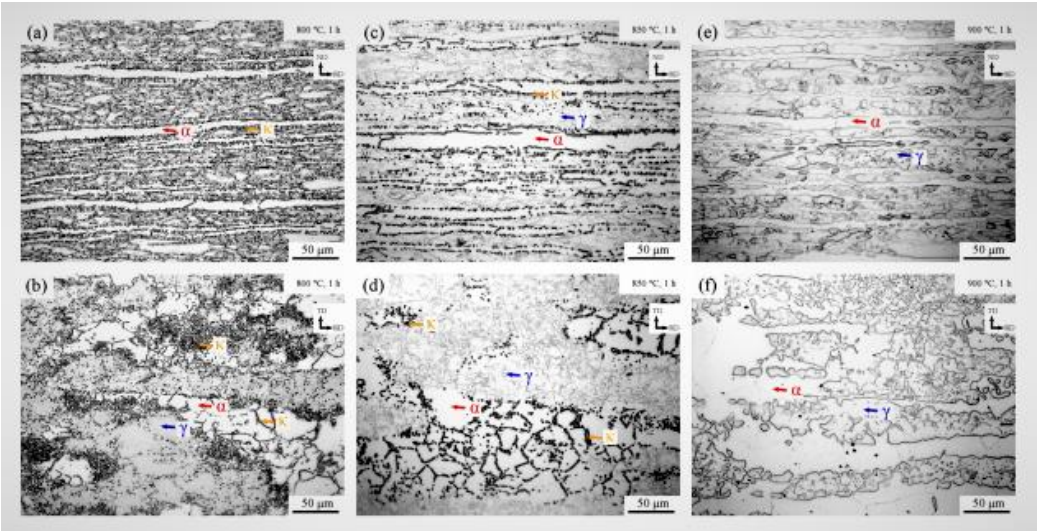


Figure 7. Optical microstructures at an annealing temperature for (a) and (b) 800°C, for (c) and (d) 850°C, for (e) and (f) 900°C [3].

From this pattern it is investigated that the κ-carbide distribution series lies between α and γ phases, whereas at a temperature of 850°C the κ-carbide phase imposed in γ phase vanishes and at 900°C a κ-carbide nearly liquefies in α and γ matrix. The outcomes for XRD measurements for each phase changes with respect to temperature have been calculated using Thermo-Calc Software and the diagram for respective is displayed below. It can be clearly seen that no transformation took place for γ phase at hardening temperature of 900°C. From figure 7, it is inspected that liquefying temperature for κ-carbide arises between 850-900°C which is far higher as calculated by Thermo-Calc displayed in Figure 8.

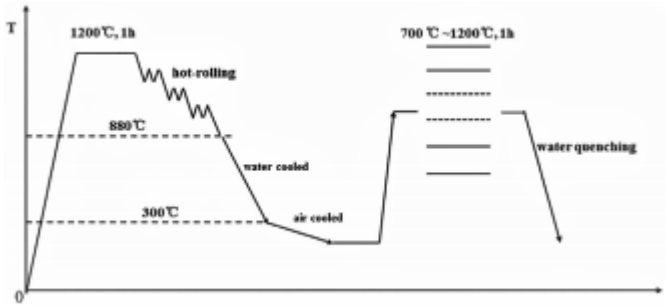


Figure 8. The rolling and annealing circumstances for a sample steel [3].

For temperature variation for annealing process from 700-900°C, the bulk division of α segment and carbide elements decreases. At 900°C, the number percentage change for fraction grades out to be 60% in all. After the cause of dissolution level, the tome fraction in γ segment increases and slightly decreases along with growth in an annealing temperature [3].

3.2 Deformation structures

The deformation structure for low density steel varies at different levels such as true strains, dislocation arrangements and its features. The phase transformation for a eutectoid reaction is shown as (γ→α + κ) which are valid for only diminutive-range facility of κ-elements. An obstruction for these particles is to be associated with a fluctuating dσ/dε curve. The dislocation formation images for different structures at a particular distance are displayed Figure 9.

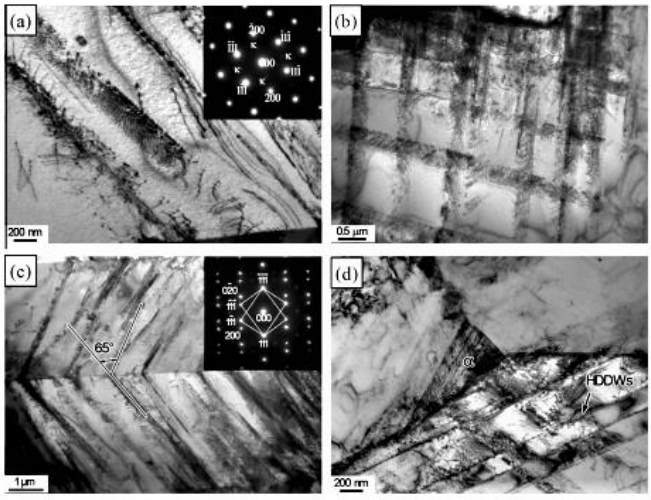


Figure 9. A dislocation pattern for models outlines (a) dislocation arrays for the structure spot, (b) intersecting at slip systems, (c) for intersecting annealing twins, (d) for high density dislocation walls (HDDWs) [1].

The dislocations sign demonstrates for visible bands for the surface of austenite grains. The further drizzle of steel quenched at a higher temperature led to the formation of an intermetallic composite which explains the hardness behavior of ferrite to be higher causing lower distortion than austenite. The dislocation conformation appears at the domain boundary region resulting out in formation of micro bands. A correlation is to be seen between slip band and dislocation organization during tensile deformation as well as gliding dislocations for the austenite phase [1]. The observation of dense dislocations is examined for a deformation zone of geometrical necessary dislocations for larger deformation. The relation between province boundary and microstructure results out to be in progress with an increase of deformation, i.e. the total dislocation density increases for increase in strain rate which contributes to improve in performance for strength and plasticity. TEM images for deformed microstructure of low density steel is shown in Figure 10.

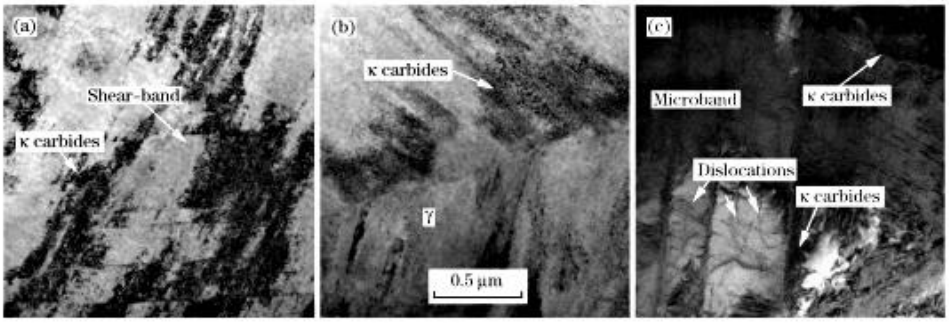


Figure 10. TEM graphs for microstructure dislocations for low density steel (a) 28Mn-12Al alloy, (b) 28Mn-10Al alloy, (c) 28Mn-8Al alloy [4].

From figure 10 the arrangements of shear ensembles can be seen for deformed 28Mn-12Al, 28Mn-10Al and 28Mn-8Al composites, respectively among which 28Mn-10Al and 28Mn-8Al alloys reveals advanced strengths and strain hardening rates due to micro groups and growth of dislocations [4].

3.3 Tensile Properties

The tensile properties for low density steel varies as of pertaining stress-strain engineering curve for specimens subjected to different tensile tests along with stress-strain curve for work hardening rate. The yielding point for work hardening rate curve occurs after a specific temperature of 700°C. The temperature for stress-strain engineering curve for annealing is so higher than that of stress-strain curve for work hardening. At an annealing temperature range of 700°- 850°C the specimens are subjected to work hardening rate that shows the reversal change in temperature for less than 5% of true strain. The curves for stress-strain engineering for tensile tests as well as curve for stress-strain for work hardening is shown in Figure 11.

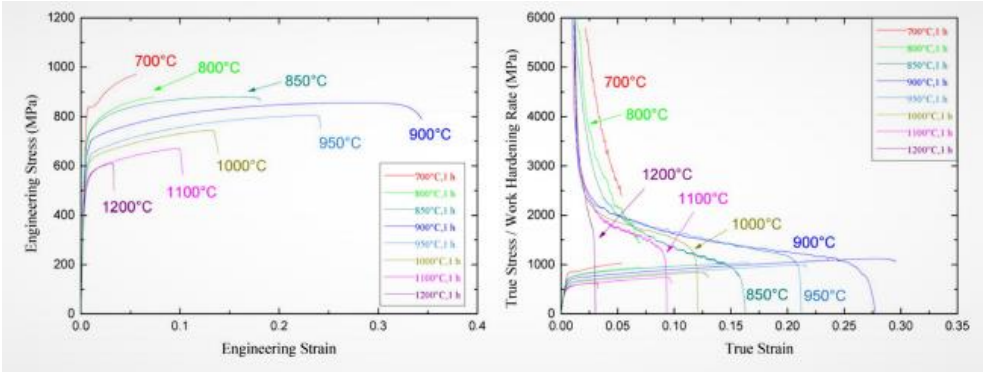


Figure 11. (a) The stress-strain curve for specimen subjected to tensile tests, (b) The stress-strain curve for work hardening rate [3].

From these curves it is seen that the ultimate strength drops with increment in an annealing temperature. An increase in annealing temperature from 700-900°C results in growth for elongating properties and further decrease with temperature rises from 900-1200°C. These changes in properties have a major impact on strength and ductile properties for steel [3].

The sampled steel undergoes annealing treatment at 650°C and 750°C at different time intervals. SEM images for the martensite phase of steel are displayed in Figure 12 for different conditions-

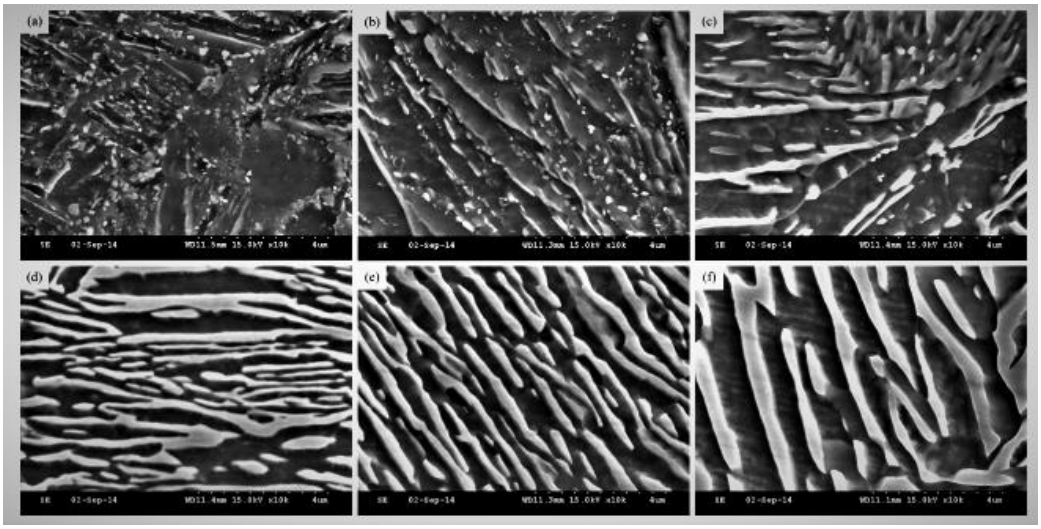


Figure 12. SEM graphs before hardening on 650°C subjected for (a) 10 min, (b) 60 min, (c) 360 min for 750°C, (d) 10 min, (e) 60 min, and (f) 360 min [5].

The drizzle and disintegration of martensite and ferrite phase is obtained at a temperature of 650°C for which these phases grew up with time. The sampled steel is hardened at 750°C that exhibits characteristics for a new ferrite and martensite phase to be in new martensite phase. With an increase in annealing time, the wideness for ferrite and martensite too increases. The increment in annealing time led to panel for Mn and Al components that are augmented in austenite and ferrite respectively. The difference in native alignment among dissimilar phases increases with hardening time [5]. The three different samples (i.e., AC, WQ, IQ) holds a higher yield as well as ultimate strengths representing a value of more than 1GPa. The overall extension to rupture (El) point is relatively short as 5% for which the freezing pattern fluctuates after AC to WQ for which the value of El becomes twice of it. The products of ultimate tensile strengths and El were used to evaluate energy captivation competence, tracing to an extreme balance of strength and ductility for IQ samples. The engineering stress-strain curves as well as a true stress-strain curve for low density steel is shown in Figure 13.

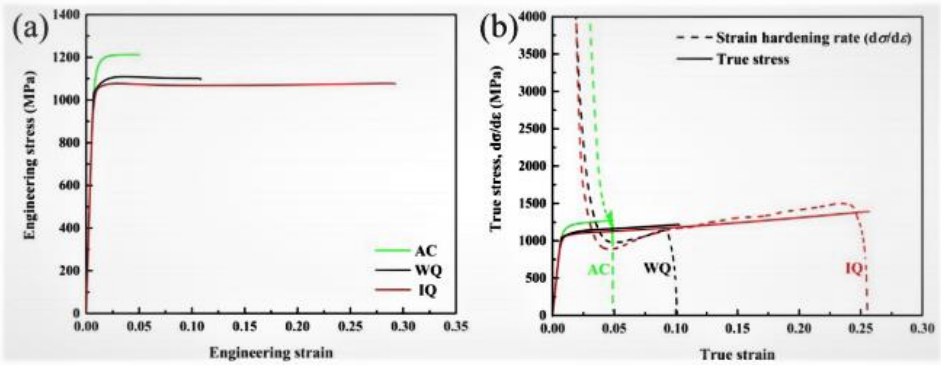


Figure 13. (a) An engineering stress-strain curve, (b) The true stress-strain curve of Air Cooling, Water Quenching, and Intensive Quenching samples [7].

The curves for true stress-strain represent the higher value for hardening rate as compared to others and the IQ samples have extreme dσ/dε principles with true tension to a larger value of strain [7].
The tensile tests for different heat treatment processes were performed for mechanical testing for production of samples. The partial transformation of austenite into ferrite in addition to κ-carbide was formed at 750°C for 2 h and 700°C for 5 h respectively. The overall alteration of ferrite and κ-carbide elements accomplished at 750°C for 5 h. The results obtained were concluded as the precipitation of an abrasive κ-carbide for the grain boundary region led to a very pitiable nature of ductility, higher grade of transformation as well as minor distortion to fracture. The plot for tensile tests subjected to different heat treatments at different temperatures are shown in Figure 14.

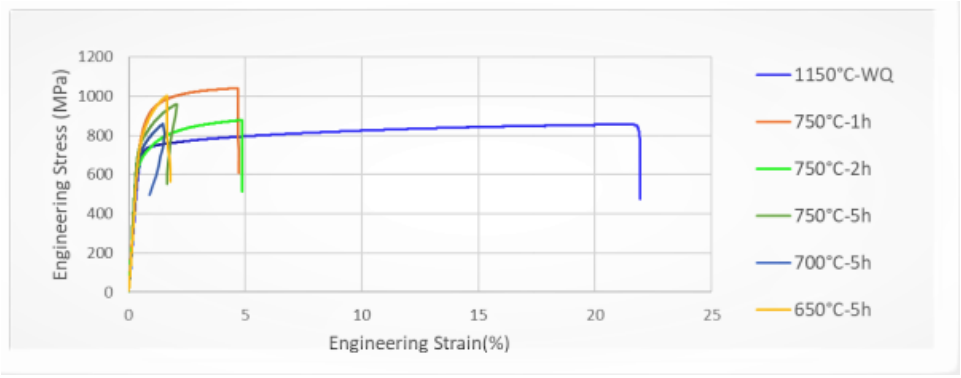


Figure 14. Ductile curves for a different heat behavior development [9].

The κ-carbide elements exhibit the high level of resistance and decrement for El as linked to quenched materials for tensile properties [9].

3.4 Hardening Behavior

The different tensile investigations curves were plotted out for strain rate ranging from 0.1-0.0001s^{-1} showing the variation in yield stress and fracture strength for which the ultimate value obtained is 400MPa for yield stress and range of 1000-1200MPa for fracture strength. It is observed that with increase in strain rate the ductility also increases which specifies the hardening and plastic behavior of materials. The work hardening rate increases for true strain of 0.15 where curves surpass at higher rates. The effect of lower strain rate and amplitude of hardening rate, the involvement of disruptions for random distributions were negotiated even though slip progressions produce high density composition in cell structure. The curves for engineering stress- strain, true stress-strain and hardening rate curves are displayed as shown in Figure 15.

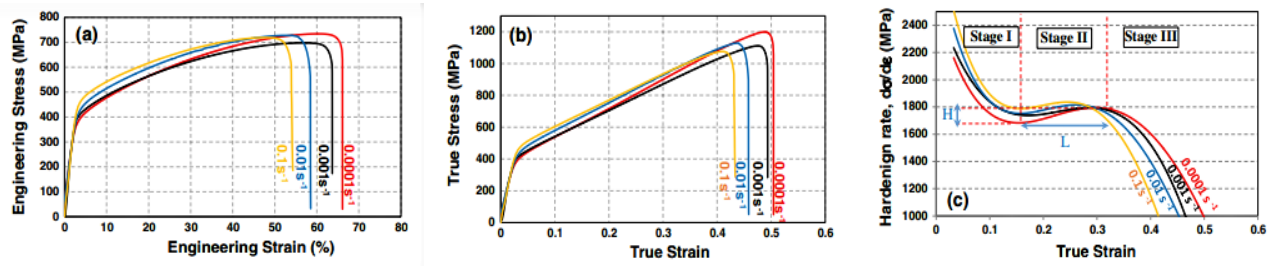


Figure 15. (a) An engineering stress-strain curve, (b) The true stress-strain curve, and (c) Hardening rate Vs True strain for the sample steel [6].

The lower strain rate promotes relaxation to dislocations by dynamic recovery up to the deformed microstructure evolved to secondary grains [6].

3.5 Fracture Characterization

The fracture analysis for two different alloy steels (28Mn-8Al and 28Mn-10Al) were indicated on behalf of their properties such as plasticity, fracture planes for two different stretchable samples presenting the nature of micro-pores at midpoint of surfaces and ductile crack. The fracture graphs for 28Mn-8Al and 28Mn-10Al steels has been displayed in Figure 16.

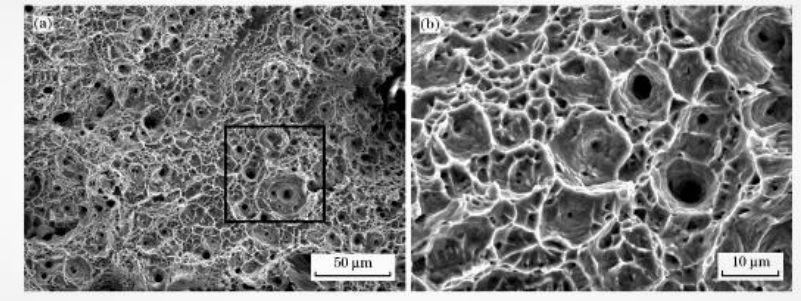


Figure 16. (a) Fracture analysis, (b) Enlarged view for 28Mn-8Al alloy steel [4].

The fracture pits for 28Mn-8Al steel having regular arrangements are uniformly distributed with larger sizes are displayed in Figure 17.

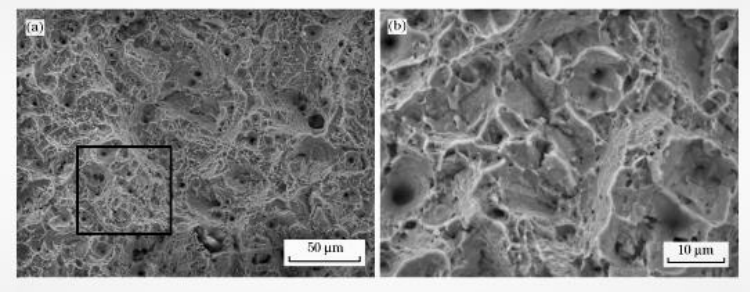


Figure 17. (a) Fracture analysis, (b) Enlarged view for 28Mn-10Al alloy steel [4].

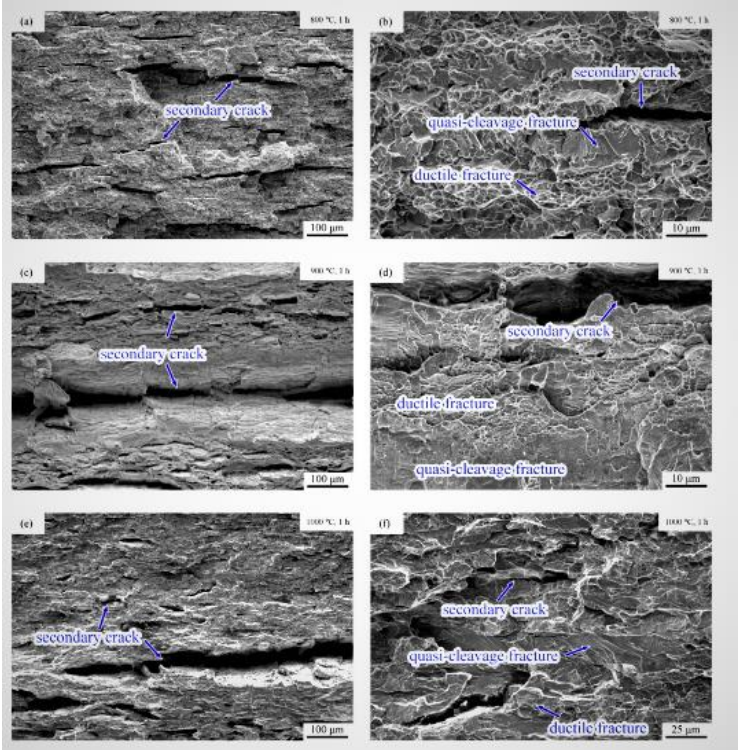


Figure 18. SEM images at temperature (a) (b) of 800°C, (c) (d) of 900°C, and (e) (f) of 1000°C [3]

The fracture pits represent for 28Mn-10Al steel having shear formation due to decrement in Al component and heaping fault energy [4]. The SEM images for fracture mode were analyzed for sample that were annealed in range from 800-1000°C for different time intervals. The propagation of fracture in specimen at 800°C shows a mixing behavior ductile fracture and quasi-separating fracture. The carbide particles are located at grain boundaries contributing to cleavage breakage for α phase. The SEM graphs are displayed in for different temperature range as shown in Figure 18.

The SEM graphs plotted at different temperatures, for which at 900°C fracture mode is predominant by mixture of γ and α phases were fracture area is spotted highly at 900°C than 1000°C. Due to the larger effect in carbide boundary grain layer along α samples were not obtained at 900°C and 1000°C [3].

The investigation for influence of cooling outline on fracture mode were made for ductile fracture that are detected by SEM as displayed as shown in Figure 19.

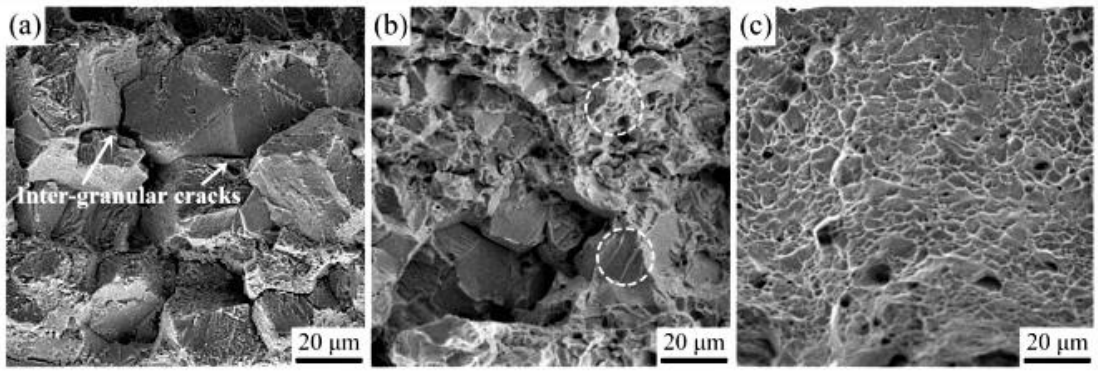


Figure 19. SEM fracture analysis of sample steel (a) for AC, (b) WQ, and (c) IQ [7].

The AC sample shows brittle nature of fracture mode as of presence of inter-granular cracks that are characterized by smooth surfaces. The fracture mechanism for WQ sample is demonstrated by narrow hollows and minor cracks led to the formation of stream pattern whereas for IQ it exhibits ductile nature, which is bidden by well-developed pits over fractured surface [7].

4. Conclusion

The phenomenon of the microstructure and its characteristics affecting the tensile properties, deformation etc. along with the fracture analysis and hardening behavior depending upon several factors as elongation to failure (El), ductility, yield strength, ultimate tensile strength with detailed explanation has been reviewed in the paper. Microstructures are related to phase transformations, grain boundaries, dislocations from which it is concluded that the κ-carbide phase transitions led to increase in microstructure, increases in grain boundary layer increases the microstructures and dislocations have minor effects on it. The several microstructural images have been shown described operating at different temperature for different conditions. The tensile and mechanical properties explains the behavior of engineering stress-strain curve as well as true stress-strain curve showing out the changes in phases and its properties respectively. The conclusion is made as with increase in annealing time the phase region too increases which led to increase in yield strength as well as ultimate tensile strength. The hardening behavior states the variation of strain rate responsible for results in fracture strength as well as tensile strength along with dislocations distributions. The conclusion is made that with increase in strain rate the ductility too increases and also the higher strain rate is responsible for progress in work hardening.

References

[1] Fuqiang Yang, Renbo Song, Yaping Li, Ting Sun, Kaikun Wang. (2015). "Tensile deformation of low- density duplex Fe–Mn–Al–C steel". Materials and Design, 76(1), 32-39.

[2] Ya-Ping Li, Ren-Bo Song, Er-Ding Wen, Fu-Qiang Yang (2016). "Hot Deformation and Dynamic Recrystallization Behavior of Austenite-Based Low-Density Fe–Mn–Al–C Steel". Acta Metallica Sin. (English Letters), 29(5), 441-449.

[3] Chao Zhao, Renbo Song, Leifeng Zhang, Fuqiang Yang, Tai Kang (2016). "Effect of annealing temperature on the microstructure and tensile properties of Fe–10Mn–10Al–0.7C low-density steel". Materials and Design, 91(1), 348-360.

[4] Xiao-fengZhang, Hao Yang, De- ping Leng, Long Zhang, Zhen-yi Huang, Guang Chen (2016). "Tensile Deformation Behavior of Fe-Mn-Al-C Low Density Steels". Journal of Iron and Steel Research, 23(9), 963-972.

[5] Mingda Zhang, Wenquan Cao, Han Dong, Jing Zhu (2016). "Element partitioning effect on microstructure and mechanical property of the micro-laminated Fe–Mn–Al–C dual phase steel". Materials Science and Engineering, 654(1), 193-202.

[6] H.R. Abedi, A. Zarei Hanzaki, Keng-Liang Ou, Chih-Hua Yu (2017). "Substructure hardening in duplex low density steel". Materials and Design, 116(1), 472-480.

[7] Degang Liu, Minghui Cai, Hua Ding, Dong Han (2018)." Control of inter/intra-granular κ-carbides and its influence on overall mechanical properties of Fe-11Mn-10Al-1.25C low density steel". Materials Science and Engineering, 715(1), 25-32.

[8] Idurre Kaltzakorta, Teresa Gutierrez, Roberto Elvira, Pello Jimbert and Teresa Guraya (2011)." Evolution of Microstructure during Isothermal Treatments of a Duplex-Austenitic 0.66C11.4Mn.9.9Al Low-Density Forging Steel and Effect on the Mechanical Properties". Metals, 11(1), 214- 227.